

Spatially-resolved spectroscopy at 1.6 μm of Titan's atmosphere and surface

M. Ádámkóvics,¹ I. de Pater,² H. G. Roe,³ S. G. Gibbard,⁴ and C. A. Griffith⁵

Received 9 March 2004; revised 19 May 2004; accepted 14 June 2004; published 18 August 2004.

[1] We present spatially-resolved, low-resolution ($\lambda/\Delta\lambda \sim 1,500$) spectroscopy of the leading hemisphere of Titan in the H-band (1.5–1.7 μm) using adaptive optics. Spatial variations of surface albedo are observed in images at 1.55–1.57 μm , which are clearly distinct from stratospheric haze. There is a significant increase in albedo around the southern (summer) pole at 1.62 μm . Using a plane-parallel radiative transfer model to fit the observed spectra, we find a 61% increase in tropopause haze opacity ($\tau = 0.100$ from 30–40 km) around the southern pole relative to the rest of the disk (where $\tau = 0.062$ from 30–40 km). **INDEX TERMS:** 0305 Atmospheric Composition and Structure: Aerosols and particles (0345, 4801); 0317 Atmospheric Composition and Structure: Chemical kinetic and photochemical properties; 0320 Atmospheric Composition and Structure: Cloud physics and chemistry; 0343 Atmospheric Composition and Structure: Planetary atmospheres (5405, 5407, 5409, 5704, 5705, 5707); 5494 Planetology: Solid Surface Planets: Instruments and techniques. **Citation:** Ádámkóvics, M., I. de Pater, H. G. Roe, S. G. Gibbard, and C. A. Griffith (2004), Spatially-resolved spectroscopy at 1.6 μm of Titan's atmosphere and surface, *Geophys. Res. Lett.*, 31, L17S05, doi:10.1029/2004GL019929.

1. Introduction

[2] The dense nitrogen-dominated atmosphere of Saturn's largest moon, Titan, has long intrigued researchers – in part because of the striking similarities to Earth's atmosphere. However, significant differences include both the lack of oxygen and the presence of CH_4 [Kuiper, 1944] as the dominant trace species, which together allow for the photochemical production of hydrocarbon aerosols. These aerosols form hazes that globally obscure the surface of Titan at visible wavelengths. In the infrared, where particle opacity becomes sufficiently low, the lower atmosphere and the surface of Titan can be observed.

[3] Advances with space-based near-infrared observing [Smith *et al.*, 1996; Meier *et al.*, 2000], ground-based speckle [Gibbard *et al.*, 1999], and adaptive optics (AO) techniques [e.g., Combes *et al.*, 1997; Coustenis *et al.*, 2001] have provided views of Titan's surface through the

haze. Narrow-band filters are used that probe spectral 'windows' in the CH_4 absorption spectrum [Griffith *et al.*, 1991] – the dominant source of near-IR opacity on Titan.

[4] Spectroscopic studies complement imaging and have long been useful in determining globally averaged vertical profiles for the various gas-phase hydrocarbons, which are the precursors to atmospheric particulates [Hunten *et al.*, 1984]. It is believed that these particulates are produced photochemically high in the stratosphere (for a review, see, e.g., McKay *et al.* [2001]), and the hazes they form have been observed to undergo seasonal changes [Lorenz *et al.*, 2001] – likely due to atmospheric circulation [Rannou *et al.*, 2002]. The particulates then settle through the stratosphere and could perhaps serve as condensation nuclei for the clouds that are regularly seen in disk-integrated spectra [Griffith *et al.*, 1998, 2000].

[5] High-spatial-resolution (AO) imaging alone [Roe *et al.*, 2002b] as well as in concert with 2 μm spectroscopy [Brown *et al.*, 2002] have led to unambiguous detections of clouds near Titan's south pole, highlighting the utility of using these two techniques in tandem. In order to investigate the properties of atmospheric particulates, we present here the first analysis of spatially-resolved 1.6 μm spectra of Titan.

2. Observations and Data Reduction

[6] Long slit (3.96'' \times 0.076'') spectra were recorded with the NIRSPEC/AO system on three nights, 19, 20, and 22 February 2001 UT, at W.M. Keck Observatory, at a spectral resolution $\lambda/\Delta\lambda \sim 1,500$. Details of the adaptive optics system may be found in, e.g., Wizinowich *et al.* [2000]. Standard procedures were used to flat field, bias and dark correct the NIRSPEC spectra. Narrowband (H1581) SCAM images of Titan were flux calibrated for normalization of the spectral image maps.

[7] While the axis along the length of the slit provides a 1-dimensional (latitudinal) spatial axis along a section of Titan's disk, the spectrometer slit must be stepped across the disk (longitudinally) to provide two spatial dimensions for the images of the disk. The full width half-maximum (FWHM) of the observed point spread function (PSF) in images was $\sim 0.050''$. In the reconstructed images the spatial resolution along the slit is $\sim 0.050''$ and perpendicular to the slit the resolution is dominated by the slit width (0.072'') resulting in a spatial resolution of $\sim 0.090''$. Multiple SCAM images (~ 5) were recorded, at each slit position, during the spectrometer exposure. The central slit position is determined by calculating the 1-dimensional first derivative of the intensity perpendicular to the long axis of the slit, and then finding the extrema, which identify the edges of the slit positioned on the disk.

[8] After stepping across the disk with the length of the slit oriented North-South (N-S), one spectrum was recorded

¹Department of Chemistry, University of California, Berkeley, California, USA.

²Department of Astronomy, University of California, Berkeley, California, USA.

³Division of Geological and Planetary Sciences, California Institute of Technology, Pasadena, California, USA.

⁴Institute of Geophysics and Planetary Physics, Lawrence Livermore National Laboratory, Livermore, California, USA.

⁵Lunar and Planetary Laboratory, University of Arizona, Tucson, Arizona, USA.

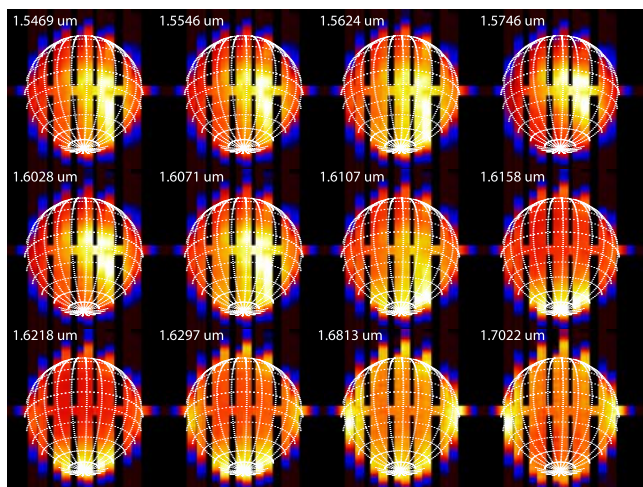


Figure 1. Spectral image maps of Titan. Each image is integrated over $0.0009 \mu\text{m}$ around the central wavelength indicated. The sub-observer point is 111°W longitude and -23°N latitude, the phase angle is $\sim 6^\circ$, and the sub-solar point is East (to the right) of the sub-observer point.

at a slit position perpendicular to the previous 10 (E-W). This spectrum is used to scale each of the 10 N-S spectra such that the signal in the regions of spatial overlap between the N-S and E-W spectra match. The spectrum taken E-W along the disk is scaled to the corresponding region of the

flux calibrated, narrowband (H1581 filter) SCAM images, with uncertainties in the photometry $\sim 15\%$.

3. Results and Discussion

3.1. Images

[9] Figure 1 shows a subset of ultra-narrowband images reconstructed from the spectra that are characteristic of the dataset. The first row of images are from $1.55\text{--}1.57 \mu\text{m}$, where CH_4 absorption is weak, and primarily intensity from the surface is measured. The dominant surface feature is the bright feature located at $\sim 100^\circ\text{W}$.

[10] The middle row of images in Figure 1 show that as CH_4 opacity increases with wavelength, flux from higher altitude in the atmosphere is observed. At $1.6028 \mu\text{m}$ the surface dominates the signal, whereas at $1.6158 \mu\text{m}$ flux from a tropopause haze is observed (see below). At wavelengths longer than $1.6158 \mu\text{m}$ the bright surface feature is no longer visible. CH_4 absorption at this wavelength is strong enough to completely attenuate the light from the sun before it reaches the surface. The observed signal is therefore from photons that are scattered from particulates in the atmosphere.

[11] The $1.6158 \mu\text{m}$ image shows that there is a localized enhancement of lower-atmospheric particulates near the southern (summer) pole. This enhancement occurs at the latitude where tropopause cirrus has been detected spectroscopically at $2.1 \mu\text{m}$ [Griffith *et al.*, 1998; Brown *et al.*, 2002] and has been directly imaged with a narrowband filter at $2.108 \mu\text{m}$ [Roe *et al.*, 2002b]. We show by modelling the

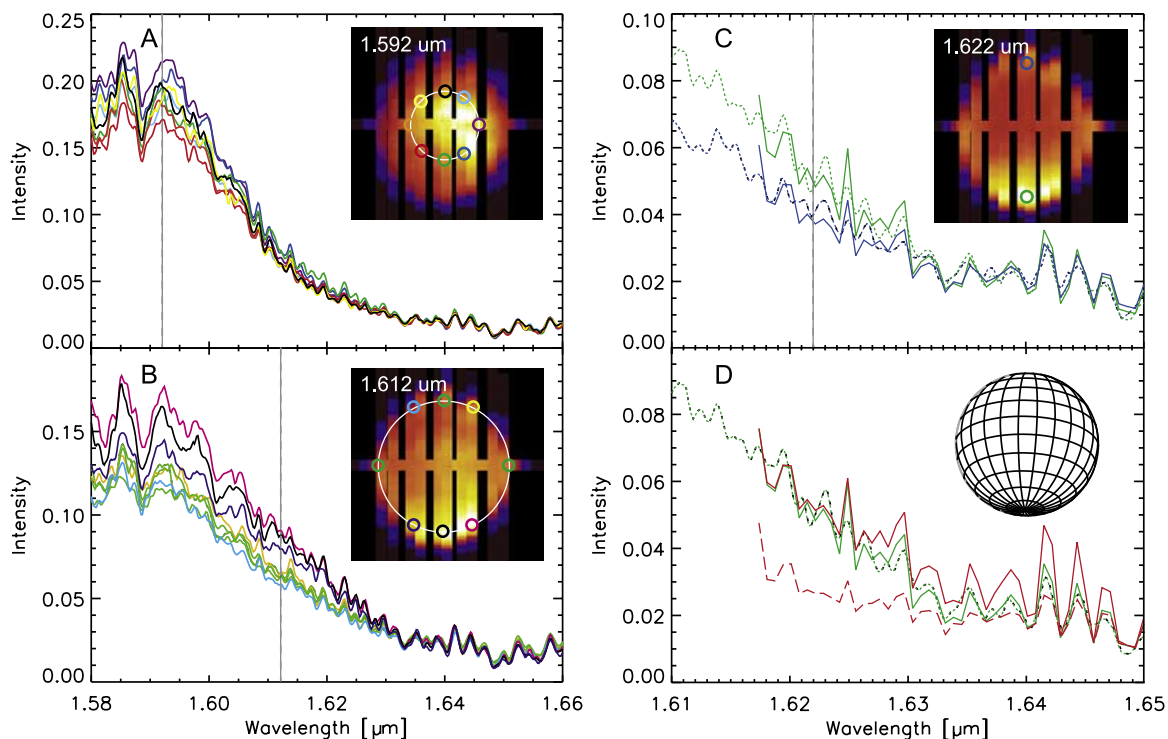


Figure 2. Observed and modeled spectra from multiple locations at the same airmass on Titan's disk – the dashed vertical lines are the wavelength of the inset images and colored circles indicate the locations of the corresponding spectra. Surface albedo contrasts that are observed at $1.592 \mu\text{m}$ (A) do not significantly affect spectra from $1.61\text{--}1.66 \mu\text{m}$. Enhanced tropopause haze at the southern limb (B) is probed from $1.61\text{--}1.62 \mu\text{m}$. Panel C compares the observed spectra (points) with radiative transfer model (lines) that fit the tropopause haze enhancement. Altitude dependence of tropopause haze (D) is more sensitive to decrease (red dashed line) to 20 km than to increase to 70 km (red solid line).

observed spectra from this region that this haze is found at 30–50 km, near the tropopause at 42 km.

[12] At wavelengths longer than 1.6218 μm (bottom row of Figure 1), stratospheric particulates are measured. At these wavelengths the observed flux is diminished, signal-to-noise decreases, and limb brightening becomes more pronounced. The N-S stratospheric haze asymmetry imaged on the same night with an H1702 narrowband filter [Roe *et al.*, 2002a] is seen in the 1.702 μm image and quantitatively modeled below. However, with the narrow bandpass and incomplete spatial coverage of these images we do not clearly observe the E-W asymmetry or polar collar seen by Roe *et al.* [2002a].

3.2. Spectra

[13] The pathlength through Titan’s atmosphere plays a critical role in determining the observed spectra. Therefore, we first compare spectra measured at the same Titan airmass – that is, points that are equidistant from the center of the disk. Figure 2a shows 8 spectra taken at a Titan airmass of $A = 1.12$ (0.5 Titan radii, R_T , from disk center). The pixel-to-pixel noise of each spectrum is read-noise limited (~ 30 DN, or in this case $0.003 I/F$) and the similarity of the spectra longward of 1.63 μm is a reassuring consistency check of the data reduction, normalization, image reconstruction and centering.

[14] Shortward of 1.60 μm the spectra diverge as they probe deeper into the troposphere. The greatest contrast in the spectra occurs at 1.592 μm , where the measurement is sensitive to surface albedo. Figure 2a shows that bright surface features show up in the spectra at 1.592 μm , and that they do not affect the spectra significantly at wavelengths longer than 1.610 μm . This qualitatively indicates that the spectra from 1.61 to 1.64 μm probe an altitude region from the troposphere to the lower stratosphere, and exclude the surface.

[15] The bright feature seen around the southern pole at 1.62 μm can be investigated by comparing spectra taken from around the limb ($A = 2.35$, $R_T = 0.9$) of Titan (Figure 2b). A striking feature in these spectra is the increasing divergence at wavelengths shorter than 1.63 μm . The five spectra from the northern hemisphere overlap at 1.61 μm , and contrast with the three spectra from the southern hemisphere at this wavelength. This indicates a robust observational difference between the two sets of spectra.

3.3. Model

[16] A 2-stream approximation solves the radiative transfer equation for plane-parallel layers [McKay *et al.*, 1989]. Line-by-line techniques are used to calculate the absorption coefficients from the methane line parameters compiled in the GEISA database [Husson *et al.*, 1991]. Particles are assumed to scatter as spherical particles, and the Voyager thermal profile is adopted [Lellouch *et al.*, 1989]. The modelled spectra cut off at 1.617 μm as limited by laboratory data for the CH_4 spectrum’s pressure and temperature dependence. This limitation sets the depth into the troposphere that is accurately modelled to 30 km. Improved laboratory data for weak CH_4 transitions in this region would allow analysis of the existing data to probe deeper into the troposphere. Currently, the rich 1.6 μm spectra corresponding to regions below 30 km, where the intriguing cloud and tropospheric haze formation occur, can only be interpreted qualitatively.

Table 1. Comparison of Altitude Dependence of Stratospheric Haze Layers in the Northern Mid Latitudes and Near the Southern Pole.

Stratospheric Haze Altitude Profiles						
Altitude (km) ^a	Pressure (mbar)	Temp (K)	25°N		80°S	
			Optical Depth	Extinction (km^{-1})	Optical Depth	Extinction (km^{-1})
179	0.001	174	0.001	3.1(–5)	0.001	3.1(–5)
150	0.002	170	0.014	5.4(–4)	0.010	3.9(–4)
130	0.003	163	0.013	1.4(–3)	0.008	9.5(–4)
110	0.006	154	0.016	2.2(–3)	0.009	1.4(–3)
90	0.010	144	0.015	3.0(–3)	0.010	1.9(–3)
70	0.020	122	0.023	4.1(–3)	0.026	3.2(–3)
50	0.052	74.1	0.046	6.4(–3)	0.074	6.9(–3)
40	0.111	71.2	0.041	1.7(–2)	0.066	2.0(–2)
30	0.207	71.5	0.062	2.3(–2)	0.100	3.0(–2)
24	0.330	73.7	—	—	—	—
Sum			0.23		0.30	

^aAltitude at the bottom of the layer in RT model.

[17] The initial estimate of the haze extinction vertical profile follows a scale height of 21 km. A rudimentary χ^2 minimization technique is used to systematically vary the relevant atmospheric parameters – the haze densities in the 9 uppermost layers, the surface albedo, and the CH_4 mixing ratio – while determining the mean deviation between the observed spectrum and model output. We fit a series of values (~ 10) for each parameter while holding all others at their initial value. The parameter adjustment that yields the smallest χ^2 is then updated, and the processes is repeated until the mean squared deviation between the model and the data is below the observation uncertainty (~ 20 –30 iterations).

[18] Since multiple solutions for the haze extinction profile give similar values for the minimum χ^2 – the extinction may be shown to be anti-correlated in neighboring layers of the model – we select for those extinction profiles that follow the atmospheric scale height with our initial estimate. Profiles that deviate significantly from an exponential decrease with altitude are rejected as unphysical. Changes of a few percent from the best fit optical depths produce modelled spectra outside of the pixel-to-pixel noise of the observations, so uncertainty in the optical depth is estimated to be $\sim 20\%$, primarily from the uncertainty in the photometry.

[19] The extinction profiles of the haze that fit the spectra in Figure 2c are shown in Table 1. The optical depth in the southern polar region from 30–40 km ($\tau_S = 0.100$) is almost double the corresponding region from the northern hemisphere ($\tau_N = 0.062$). At higher altitude in the stratosphere (90–150 km) the haze optical depth is greater in the North than in the South, which is in agreement with narrowband images at 1.702 μm [Roe *et al.*, 2002a]. The total haze optical depths in both the North and South agree with values derived from 2 μm images [Gibbard *et al.*, 2004].

[20] The best fit profiles follow the atmospheric number density scale height [Yelle *et al.*, 1997], $h = 18$ km from 0–60 km and $h = 35$ km from 80–200 km. This is in general consistent with current microphysical models of particle settling [McKay *et al.*, 2001; Luz *et al.*, 2003] and consistent with extinction profiles determined from modelling 0.89–0.95 μm narrowband HST images [Young *et al.*, 2002].

[21] Sensitivity tests for the altitude of the lower-stratospheric haze layers, in particular the altitude of the enhance-

ment in the southern hemisphere, are shown in Figure 2d. Systematically shifting the haze opacity parameters down by one layer clearly under-predicts the signal at 1.62 μm and the slope of the spectrum as it increases toward shorter wavelengths. Exchanging the values for haze opacity at 30 and 40 km – representing a haze enhancement higher in the atmosphere – is a much more subtle effect, but nonetheless produces a spectrum that is outside of the observational error. This indicates that while the observed haze may extend slightly below the tropopause, it does not extend deep into the troposphere, and is more likely to be distributed about the tropopause (at 42 km) and above.

[22] The distinct drop in haze opacity below 30 km observed by *Young et al.* [2002] is not readily tested with the analysis presented here. While clearing of aerosols by rainout may occur below 30 km, minor changes to the extinction profile (Figure 2d) produce results outside of the observational uncertainty, suggesting that the atmosphere at the south pole is not cleared up to 80 km [*McKay et al.*, 2001].

[23] It's not clear what concentrates Titan's particles in Titan's southern tropopause. The particles that we witness lie above the daily cumuli that appear at Titan's south pole. These particles reside at altitudes similar to those observed at 2 μm [*Bouchez*, 2003] and at 0.7–1.0 μm (C. A. Griffith et al., Imaging temporal changes on Titan, submitted to *Icarus*, 2004). Potentially they are related to the discrete clouds and form from the same updrafts that may form the lower clouds. Another possibility is that they represent haze concentrated dynamically by Titan's circulation [*Rannou et al.*, 2003]. Alternatively we may be observing the condensation of ethane on settling particles, which occurs above that of methane [*Barth and Toon*, 2003, 2004].

4. Conclusions

[24] As field integral spectrometers come online, it will be possible to regularly produce datacubes such as the one presented here for monitoring of the seasonal variations (29.5 year cycles) in the 3-dimensional spatial distribution of haze and clouds. Such information will be necessary to test models that couple circulation and the photochemical formation of aerosols on Titan. Remote observations will remain necessary to have a dynamical understanding of Titan's atmosphere, even after detailed measurements are made possible by the arrival of the Cassini spacecraft to Titan on its 4 year mission.

[25] **Acknowledgments.** The data were obtained at the W. M. Keck Observatory, which is operated as a scientific partnership among the California Institute of Technology, the University of California and the National Aeronautics and Space Administration. The Observatory was made possible by the generous financial support of the W. M. Keck Foundation. This particular study was partially supported by the National Science Foundation and Technology Center for Adaptive Optics, grant no. AST-0205893, managed by the University of California at Santa Cruz under cooperative agreement No. AST-9876783.

References

Barth, E. L., and O. B. Toon (2003), Microphysical modeling of ethane ice clouds in Titan's atmosphere, *Icarus*, 162, 94–113.
 Barth, E. L., and O. B. Toon (2004), Properties of Titan's methane-ethane clouds from microphysical modeling (abstract), *Bull. Am. Astron. Soc.*, 35(4), 927.
 Bouchez, A. H. (2003), Seasonal trends in Titan's atmosphere: Haze, wind, and clouds, Ph.D. thesis, Calif. Inst. of Technol., Pasadena, Calif.
 Brown, M. E., A. H. Bouchez, and C. A. Griffith (2002), Direct detection of variable tropospheric clouds near Titan's south pole, *Nature*, 420, 795–797.

Combes, M., L. Vapillon, E. Gendron, A. Coustenis, O. Lai, R. Witteberg, and R. Sirdy (1997), Spatially resolved images of Titan by means of adaptive optics, *Icarus*, 129, 482–497.
 Coustenis, A., et al. (2001), Images of Titan at 1.3 and 1.6 μm with adaptive optics at the CFHT, *Icarus*, 154, 501–515.
 Gibbard, S. G., B. Macintosh, D. Gavel, C. E. Max, I. de Pater, A. M. Ghez, E. F. Young, and C. P. McKay (1999), Titan: High-resolution speckle images from the Keck Telescope, *Icarus*, 139, 189–201.
 Gibbard, S. G., I. de Pater, B. A. Macintosh, H. G. Roe, C. E. Max, E. F. Young, and C. P. McKay (2004), Titan's 2 μm surface albedo and haze optical depth in 1996–2004, *Geophys. Res. Lett.*, 31, L17S02, doi:10.1029/2004GL019803.
 Griffith, C. A., T. Owen, and R. Wagener (1991), Titan's surface and troposphere, investigated with ground-based, near-infrared observations, *Icarus*, 93, 362–378.
 Griffith, C. A., T. Owen, G. A. Miller, and T. Geballe (1998), Transient clouds in Titan's lower atmosphere, *Nature*, 395, 575–578.
 Griffith, C. A., J. L. Hall, and T. R. Geballe (2000), Detection of daily clouds on Titan, *Science*, 290, 509–513.
 Hunten, D. M., M. G. Tomasko, F. M. Flasar, R. E. Samuelson, D. F. Strobel, and D. J. Stevenson (1984), Titan, in *Saturn*, edited by T. Gehrels and M. Shapley Matthews, pp. 671–759, Univ. of Ariz. Press, Tucson.
 Husson, N., B. Bonnet, N. A. Scott, and A. Chedin (1991), The GEISA data bank 1991 version, *Internal Note, L.M.D. 163*, Lab. de Meteorol. Dyn., Palaiseau, France.
 Kuiper, G. P. (1944), Titan: A satellite with an atmosphere, *Astrophys. J.*, 100, 378–383.
 Lellouch, E., A. Coustenis, D. Gautier, F. Raulin, N. Dubouloz, and C. Frere (1989), Titan's atmosphere and hypothesized ocean: A reanalysis of the Voyager 1 radio-occultation and IRIS 7.7-micron data, *Icarus*, 79, 328–349.
 Lorenz, R. D., E. F. Young, and M. T. Lemmon (2001), Titan's smile and collar: HST observations of seasonal change 1994–2000, *Geophys. Res. Lett.*, 28, 4453–4456.
 Luz, D., F. Hourdin, P. Rannou, and S. Lebonnois (2003), Latitudinal transport by barotropic waves in Titan's stratosphere: II. Results from a coupled dynamics-microphysics-photochemistry GCM, *Icarus*, 166, 343–358.
 McKay, C. P., J. B. Pollack, and R. Courtin (1989), The thermal structure of Titan's atmosphere, *Icarus*, 80, 23–53.
 McKay, C. P., A. Coustenis, R. E. Samuelson, M. T. Lemmon, R. D. Lorenz, M. Cabane, P. Rannou, and P. Drossart (2001), Physical properties of the organic aerosols and clouds on Titan, *Planet. Space Sci.*, 49, 79–99.
 Meier, R., B. A. Smith, T. C. Owen, and R. J. Terrile (2000), The surface of Titan from NICMOS observations with the Hubble Space Telescope, *Icarus*, 145, 462–473.
 Rannou, P., F. Hourdin, and C. P. McKay (2002), A wind origin for Titan's haze structure, *Nature*, 418, 853–856.
 Rannou, P., C. P. McKay, and R. D. Lorenz (2003), A model of Titan's haze of fractal aerosols constrained by multiple observations, *Planet. Space Sci.*, 51, 963–976.
 Roe, H. G., I. de Pater, B. A. Macintosh, S. G. Gibbard, C. E. Max, and C. P. McKay (2002a), NOTE: Titan's atmosphere in late southern spring observed with adaptive optics on the W. M. Keck II 10-Meter Telescope, *Icarus*, 157, 254–258.
 Roe, H. G., I. de Pater, B. A. Macintosh, and C. P. McKay (2002b), Titan's clouds from Gemini and Keck adaptive optics imaging, *Astrophys. J.*, 581, 1399–1406.
 Smith, P. H., M. T. Lemmon, R. D. Lorenz, L. A. Sromovsky, J. J. Caldwell, and M. D. Allison (1996), Titan's surface, revealed by HST imaging, *Icarus*, 119, 336–349.
 Wizinowich, P., et al. (2000), First light adaptive optics images from the Keck II Telescope: A new era of high angular resolution imagery, *Publ. Astron. Soc. Pac.*, 112, 315–319.
 Yelle, R. V., et al. (1997), The Yelle Titan atmosphere engineering models, in *Huygens: Science, Payload and Mission, Eur. Space Agency Spec. Publ.*, ESA-SP 1177, 243–256.
 Young, E. F., P. Rannou, C. P. McKay, C. A. Griffith, and K. Noll (2002), A three-dimensional map of Titan's tropospheric haze distribution based on Hubble Space Telescope imaging, *Astron. J.*, 123, 3473–3486.

M. Ádámkóvics, Department of Chemistry, University of California, Latimer Hall, Berkeley, CA 94720-1460, USA. (mate@haze.cchem.berkeley.edu)

I. de Pater, Department of Astronomy, University of California, Berkeley, CA, USA.

S. G. Gibbard, Institute of Geophysics and Planetary Physics, Lawrence Livermore National Laboratory, Livermore, CA, USA.

C. A. Griffith, Lunar and Planetary Laboratory, University of Arizona, Tucson, AZ, USA.

H. G. Roe, Division of Geological and Planetary Sciences, California Institute of Technology, Pasadena, CA, USA.